

## LA-UR-15-29260

Approved for public release; distribution is unlimited.

Title: Simulation evaluation of NIST air-kerma rate calibration standard for electronic brachytherapy

Author(s): Hiatt, Jessica R.  
Rivard, Mark J.  
Hughes, Henry Grady III

Intended for: Medical Physics

Issued: 2015-12-02

---

**Disclaimer:**

Los Alamos National Laboratory, an affirmative action/equal opportunity employer, is operated by the Los Alamos National Security, LLC for the National Nuclear Security Administration of the U.S. Department of Energy under contract DE-AC52-06NA25396. By approving this article, the publisher recognizes that the U.S. Government retains nonexclusive, royalty-free license to publish or reproduce the published form of this contribution, or to allow others to do so, for U.S. Government purposes. Los Alamos National Laboratory requests that the publisher identify this article as work performed under the auspices of the U.S. Department of Energy. Los Alamos National Laboratory strongly supports academic freedom and a researcher's right to publish; as an institution, however, the Laboratory does not endorse the viewpoint of a publication or guarantee its technical correctness.

# Simulation evaluation of NIST air-kerma rate calibration standard for electronic brachytherapy

Jessica R. Hiatt

Biomedical Engineering and Biotechnology, University Massachusetts Lowell, Lowell, Massachusetts 01854

Mark J. Rivard

Department of Radiation Oncology, Tufts University School of Medicine, Boston, Massachusetts 02111

H. Grady Hughes

Los Alamos National Laboratory, Los Alamos, New Mexico 87545

**Purpose:** Dosimetry for the model S700 50 kV electronic brachytherapy (eBT) source (Xoft, Inc., a subsidiary of iCAD, San Jose, CA) was simulated using Monte Carlo (MC) methods by Rivard *et al.* [Med. Phys. **33**, 4020–4032 (2006)] and recently by Hiatt *et al.* [Med. Phys. **42**, 2764–2776 (2015)] with improved geometric characterization. While these studies examined the dose distribution in water, there have not previously been reports of the eBT source calibration methods beyond that recently reported by Seltzer *et al.*, [J. Res. Natl. Inst. Stand. Technol. **108**, 337–357 (2003)]. Therefore, the motivation for the current study was to provide an independent determination of air-kerma rate at 50 cm in air  $\dot{K}_{\text{air}}(d = 50 \text{ cm})$  using MC methods for the model S700 eBT source.

**Methods:** Using CAD information provided by the vendor and disassembled sources, an MC model was created for the S700 eBT source. Simulations were run using the MCNP6 radiation transport code for the NIST Lamperti air ionization chamber according to specifications by Boutillion *et al.* [Metrologia **5**, 1–11 (1969)], in air without the Lamperti chamber, and in vacuum without the Lamperti chamber.  $\dot{K}_{\text{air}}(d = 50 \text{ cm})$  was determined using the \*F4 tally with NIST values for the mass energy-absorption coefficients for air. Photon spectra were evaluated over  $2\pi$  azimuthal sampling for polar angles of  $0^\circ \leq \theta \leq 180^\circ$  every  $1^\circ$ . Volume averaging was averted through tight radial binning. Photon energy spectra were determined over all polar angles in both air and vacuum using the F4 tally with 0.1 keV resolution. A total of  $10^{11}$  simulated histories were run for the Lamperti chamber geometry (statistical uncertainty of 0.14%), with  $10^{10}$  histories for the in-air and in-vacuum simulations (statistical uncertainty of 0.04%). The total standard uncertainty in the calculated air-kerma rate determination amounted to 6.8%.

**Results:** MC simulations determined the air-kerma rate at 50 cm from the source with the modeled Lamperti chamber to be  $(1.850 \pm 0.126) \times 10^{-4}$  Gy/s, which was within the range of  $\dot{K}_{\text{air}}(d = 50 \text{ cm})$  values  $(1.67 \text{ to } 2.11) \times 10^{-4}$  Gy/s measured by NIST. The ratio of the photon spectra in air and in vacuum were in good agreement above 13 keV, and for  $\theta < 150^\circ$  where the influence of the Kovar sleeve and the Ag epoxy components caused increased scatter in air. Below 13 keV, the ratio of the photon spectra in air to vacuum exhibited a decrease that was attributed to increased attenuation of the photons in air. Across most of the energy range on the source transverse plane, there was good agreement between our simulated spectra and that measured by NIST. Discrepancies were observed above 40 keV where the NIST spectrum had a steeper fall-off towards 50 keV.

**Conclusion:** Through MC simulations of radiation transport, this study provided an independent validation of the measured air-kerma rate at 50 cm in air at NIST for the model S700 eBT source, with mean results in agreement within 3.3%. This difference was smaller than the range (i.e., 23%) of the measured values.

Key words: electronic brachytherapy, calibration, MCNP6

## 1. INTRODUCTION

### 1.A. Description of eBT source

Compared to conventional radionuclide-based brachytherapy, electronic brachytherapy (eBT) offers several advantages. Given photon emission  $> 50$  keV, treatments can be delivered in an unshielded room in contrast to the substantial shielding required for high-dose-rate (HDR)  $^{192}\text{Ir}$  brachytherapy sources. When shielded, the low exposure rate allows staff to remain near the patient during dose delivery, and provides an opportunity to offer comfort and encouragement while in close proximity to the patient. It also facilitates installation at satellite clinics, mobile services, or rural locations that lack heavily shielded rooms. A dose rate close to that of HDR  $^{192}\text{Ir}$  can be administered with an eBT source. However, it provides a more targeted dose distribution with more rapid dose fall-off, resulting in significantly less dose to healthy tissues beyond the target region.

Xoft, Inc., a subsidiary of iCAD, Inc. (San Jose, CA), introduced their eBT system in 2006. The Xoft eBT source (model S700) is water-cooled and operates at 50 kV. The model S700 source was dosimetrically characterized by Rivard *et al.*<sup>1</sup> This work determined its brachytherapy dosimetry parameters as required in the American Association of Physicists in Medicine (AAPM) Task Group no. 43 (TG-43) report for use in clinical treatment planning systems (TPS) for calculating patient doses.<sup>2</sup> The Radiation Calibration Laboratory at the University of Wisconsin (Madison, WI) is an Accredited Dosimetry Calibration Laboratory (ADCL) that has provided calibration coefficients for converting exposure to air-kerma strength ( $S_K$ ), traceable to a calibrated model 6711  $^{125}\text{I}$  seed, as required for calibrating well chambers used in a hospital setting.<sup>3</sup>

### 1.B. NIST eBT calibration standard

In 2014, Seltzer and colleagues published their work establishing the NIST  $\dot{K}_{\text{air}}(d = 50 \text{ cm})$  calibration standard for the model S700 eBT source operating at 50 kV and 300  $\mu\text{A}$ .<sup>4</sup> The group embarked on this work in part because suitable facilities for using a NIST standard FAC had previously been lacking. At the NIST eBT calibration facility, the model S700 source was aligned vertically and positioned between a HPGc spectrometer and the Lamperti free air chamber. The spectrometer was used to measure the photon spectrum for determination of some of the calibration correction factors. The Lamperti chamber is a parallel-plate air ionization chamber that operates at 10 kV to 50 kV and uses a guard-ring system to provide a uniform electric field within the collecting volume. It has a 0.5 cm diameter W-alloy collimator, a 1.0 cm long collector length, a 5.0 cm collector width, a 4.0 cm vertical separation between electrodes, and a 4.0 cm attenuation length within the chamber as described by Boutillon *et al.*<sup>5</sup> Over the 4.0 cm of air from the W-alloy collimator to the collecting volume, Seltzer *et al.* calculated  $k_{\text{att}} = 1.0087$  for air attenuation from the beam-defining aperture to the center of the collecting volume.

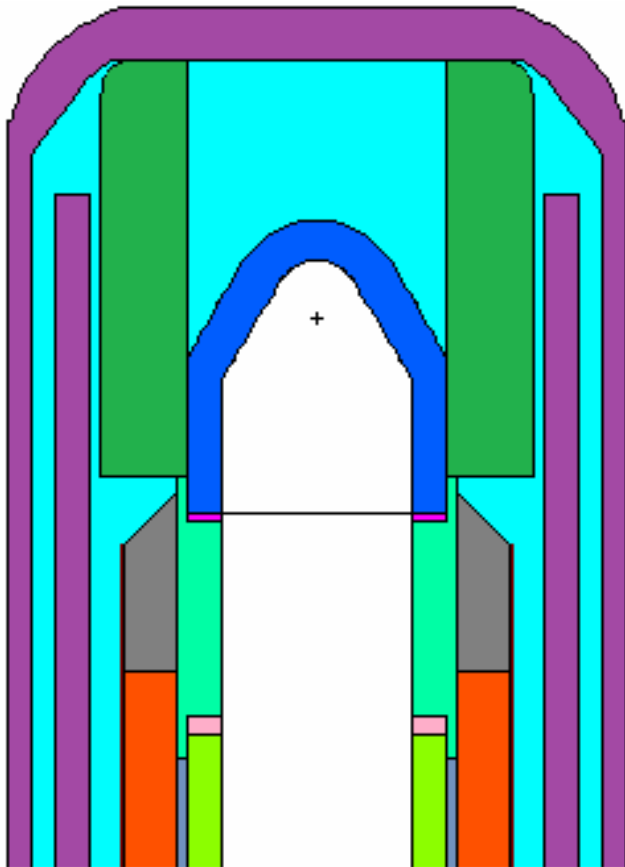


Fig. 1. Lateral view of the simulated eBT source (model S700) through a 45° sagittal plane with the crosshair positioned at the origin. The plastic anode centering insert is pictured in dark green and the Ag epoxy is pictured in grey.

### 1.C. Study rationale

After publication of the TG-43 brachytherapy dosimetry parameters but prior to clinical use,<sup>1</sup> the manufacturer modified the model S700 source design most notably to include a plastic anode-centering insert intended to improve anode centering within the source shaft and to improve coolant flow. Other design

changes included alterations in the outer plastic sheath material. Absent from the 2006 source model, but present in the current model was the Ag epoxy (Fig. 1). Dosimetry parameters for the model S700 eBT source design were reevaluated with these design changes.<sup>6</sup> Also, a new dose calculation formalism has been proposed for all eBT sources given their incompatibility with current TPSs.<sup>7</sup> The proposed formalism utilized the NIST  $\dot{K}_{\text{air}}(d = 50 \text{ cm})$  calibration standard instead of air-kerma strength. Given the advancements in source calibrations, dosimetry parameters, and dosimetry formalism, the objective of the current study was to independently evaluate the NIST eBT calibration standard using the Lamperti chamber and the reevaluated model S700 source design for a theoretical assessment of  $\dot{K}_{\text{air}}(d = 50 \text{ cm})$  values.

## 2. MATERIALS AND METHODS

### 2.A. General MC approach

The MCNP6 radiation transport code (version 1.0) was used to simulate the model S700 eBT source and the Lamperti chamber geometry.<sup>8</sup> All of the simulations were performed with coupled photon/electron transport (MODE P E) rather than the more approximate photon-only method (MODE P). The recently available single event method for electron transport has an improved ability to simulate electron impact ionization for generating L-edge fluorescence x rays in comparison to the condensed history method. Results presented herein are for the single event method unless otherwise specified. The EPRDATA12 photo/electroatomic cross section library<sup>9</sup> was used to govern the radiation interactions,<sup>10,11</sup> which included detailed treatments of K shell and L shell x-ray transitions previously not available in MCNP5 simulations. This cross section library was based on the Evaluated Nuclear Data File/B version VI Release 8 (ENDF/B-VI.8),<sup>12</sup> which in turn was based on work by Cullen and his collaborators.<sup>13,14,15</sup> Photon and electron cut-off energies were set to 1 keV by default, and the default settings on the physics photon card were used. The default MCNP6 energy straggling logic (DBCN(18)=2 for “detailed straggling”) was selected over the ITS-style logic (DBCN(18)=1),<sup>10,16</sup> which was previously preferred for MCNP5.<sup>17,18</sup> It was determined that using the MCNP6 default energy indexing decreased the overall bremsstrahlung yield by about 4% in comparison to the ITS-style energy indexing. The default number of electron substeps was used for all the materials, being 12 for the W-alloy target. Using the older ITS-style energy indexing in water for 0.1 MeV electrons, sensitivity to choice of electron substeps could change the simulated result by over 10%.<sup>18</sup> The Visual Editor<sup>TM</sup> software was employed to graphically examine the simulation geometry.<sup>19</sup> To decrease the total computing time, simulations were performed on an 8-CPU cluster with different pseudo-random number seeds.<sup>20</sup> Simulations in air and vacuum that estimated photon fluence with  $2\pi$  azimuthal sampling were performed for a total of  $10^{10}$  histories. For simulations of the Lamperti chamber, a total of  $10^{11}$  histories were obtained in about two weeks.

### 2.B. Source modeling

The source geometry was coded as depicted in Fig. 1 using the Visual Editor software.<sup>19</sup> A polar angle  $\theta = 0^\circ$  points towards the distal end of the source and  $\theta = 180^\circ$  towards the proximal end (i.e., source connector). Symmetry about the source long axis (Z)

was assumed with the exception of the anode-centering insert. The source was modeled similarly as the 2015 source model,<sup>6</sup> with components including the W-alloy film (0.8  $\mu\text{m}$  thick, 14.56  $\text{g}/\text{cm}^3$ ) inside the anode (0.35 mm thick, 3.26  $\text{g}/\text{cm}^3$ ) and substrate, wall materials, and a water cooling sheath. The cooling sheath outer diameter was 5.3 mm. In addition to the plastic anode centering insert, the more recent simulation model<sup>6</sup> included Ag epoxy and the outer sheath material changed from polyether block amide<sup>1</sup> to a high-density polyethylene with a mass density of 0.95  $\text{g}/\text{cm}^3$ . The Ag epoxy was always present in the physical sources, but was not included in the simulations by Rivard *et al.*<sup>1</sup> The coordinate system origin was placed at the center of the x-ray anode cone, corresponding to the longitudinal position indicated by the black line on the outside of catheter. To establish this new simulation model, design information was taken from photomicroscopy of dissected model S700 sources and vendor-supplied CAD drawings.<sup>6</sup> The complex shape of the centering insert is proprietary, but the minimum and maximum thicknesses of this plastic insert were 0.34 mm and 0.75 mm, respectively, which were the same as the values used by Davis.<sup>21</sup>

## 2.C. Simulation geometries

Simulations were performed for three geometries:

- (1) source in air, with the Pb shield and the Lamperti chamber fully modeled,
- (2) source in air, without the Pb shield or the Lamperti chamber present, and
- (3) source in vacuum, without the Pb shield or the Lamperti chamber present.

The last two simulation geometries evaluated air kerma in a 200 cm radius sphere at distances of 50, 54, 100, and 150 cm from the model S700 source between two planes positioned  $\pm 0.25$  cm from the model S700 transverse plane. The tally volumes were all 0.5 cm high. To yield air kerma, the \*F4 tally (energy fluence in a cell) was used with mass energy-absorption coefficients for air taken from NIST,<sup>22</sup> assuming the equivalence of mass energy-absorption coefficients and mass energy-transfer coefficients. Photon spectra were sampled over  $2\pi$  azimuthal sampling from  $0^\circ$  to  $180^\circ$  every  $1^\circ$ . Tight radial binning was also used to prevent volume averaging, with a 0.1 nm bin thickness. Photon energy spectra were determined using the F4 tally (photon flux in a cell) with 0.1 keV resolution.

### 2.C.1. Lamperti chamber

Adapted from Seltzer *et al.*,<sup>4</sup> a photograph of the NIST measurement geometry is shown in Fig. 2(a). The first simulation geometry modeled the NIST measurement geometry using the Lamperti chamber in air as described by Seltzer *et al.*<sup>4</sup> The dry air was composed of N, O, Ar, and C in mass proportions of 75.5267%, 23.1781%, 1.2827%, and 0.124%, respectively,<sup>22</sup> with a mass density of 1.196  $\text{mg}/\text{cm}^3$ . To minimize contributions of radiation scatter in the room to the measured result, Seltzer *et al.*<sup>4</sup> used a 0.635 cm ( $1/4''$ ) thick Pb collimator having a 3.6 cm diameter aperture, positioned 37 cm from the model S700 source. To reflect the physical circumstances, simulation of the Lamperti chamber aperture was 0.5 cm in diameter; positioned 50 cm from the center of the model S700 source; with an assumed collimator composition of W, Ni, and Fe in mass proportions of 90%, 6%, and 4%, respectively, and a mass density of 17  $\text{g}/\text{cm}^3$ . For

comparison with Fig. 2(a), a graphical depiction of the simulated measurement geometry is given in Fig. 2(c) and Fig. 2(d).

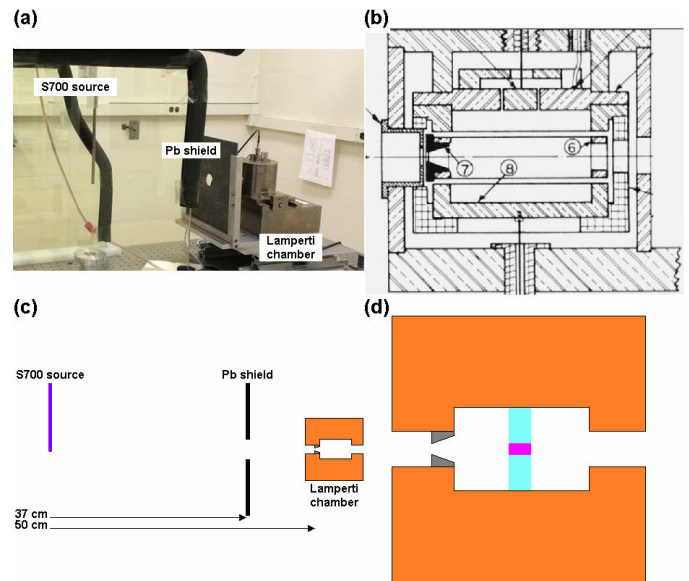


**Fig. 2.** (a) The NIST  $\dot{K}_{\text{air}}(d = 50 \text{ cm})$  measurement geometry of the model S700 electronic brachytherapy source, as adapted from Fig. 7 of Seltzer *et al.*<sup>4</sup> The relative positions of the source, Pb shield, and the Lamperti air ionization chamber are shown. (b) Schematic diagram of the Lamperti air ionization chamber from Fig. 6a of Boutillon *et al.*<sup>5</sup> Parts (a) and (b) are reprinted courtesy of the National Institute of Standards and Technology, U.S. Department of Commerce (not copyrightable in the United States). Simulation of the NIST measurement geometry is depicted in a sagittal plane by the Visual Editor<sup>TM</sup> software. (c) The Pb shield (0.635 cm thick, 3.6 cm aperture) and front face of the W-alloy collimator (grey) are 37 cm and 50 cm from the source, respectively. (d) The NIST Lamperti chamber brass shell (orange), W-alloy collimator (grey), collecting volume (blue), and the irradiated fraction of the collecting volume (fuchsia) defined by the W-alloy collimator and the collecting electrode.

The Lamperti chamber geometry was simulated according to design specifications from Boutillon *et al.*<sup>5</sup> as described by Seltzer *et al.*<sup>4</sup> A schematic representation of the Lamperti chamber is shown in Fig. 2(b). The chamber material was brass, with assumed mass compositions of 65% Cu and 35% Zn, and a mass density of 8.65  $\text{g}/\text{cm}^3$ . The path length from the W-alloy collimator to the center of the chamber internal dimensions was 4 cm. The collecting electrode was 1.0135 cm along the beam direction. The F4 and \*F4 tallies were used to estimate the photon spectra and the air-kerma rate, respectively, within the chamber collecting volume, see Fig. 2(d).

The value of  $\dot{K}_{\text{air}}(d = 50 \text{ cm})$  was obtained using Eq. (1) by correcting the raw simulated results  $M$  for  $k_{\text{att}}$ , photon scatter in air  $k_{\text{sc}}$ , and the volume of the sampling cell that was irradiated  $k_{\text{vol}}$ ,

$$\dot{K}_{\text{air}}(d = 50 \text{ cm}) = M \cdot k_{\text{att}} \cdot k_{\text{sc}} \cdot k_{\text{vol}} \quad (1)$$

Results from MC simulations in units of  $\text{MeV}/(\text{g}\cdot\text{history})$  were converted to  $\text{Gy}/\text{s}$  for 300  $\mu\text{A}$  using a factor of  $3 \times 10^5$ . The calculated values for  $k_{\text{att}}$  and  $\dot{K}_{\text{air}}(d = 50 \text{ cm})$  were compared to those obtained by NIST.<sup>4,23</sup> There is a small contribution to the total air-kerma of Compton interactions which occur in air in the diaphragm and the Lamperti chamber and cause resulting scattered photons to pass through the tally region. In the

measurement standard, this contribution is removed by applying a correction.<sup>4</sup> A value of  $k_{sc} = 0.9987$  was used to correct the simulated kerma value for photon scatter in air.

### 2.C.2. Air

To understand the influence of air attenuation in the NIST measurement geometry, the second simulation geometry positioned the model S700 source centered in a sphere of dry air.

### 2.C.3. Vacuum

The third simulation geometry was identical to the second, except that the medium surrounding the source was vacuum.

## 2.D. Uncertainty analysis

As recommended in the joint AAPM/ESTRO Task Group 138 report,<sup>24</sup> an uncertainty analysis was performed to identify and quantify Type A (i.e., statistical) and Type B (i.e., non-statistical) components that contributed to derivation of  $\dot{K}_{air}(d = 50 \text{ cm})$ .

In their work establishing an eBT  $\dot{K}_{air}(d = 50 \text{ cm})$  calibration standard, Seltzer *et al.* analyzed 17 sources of uncertainties influencing their experimental measurement setup.<sup>4</sup> Type A uncertainties included the standard deviation of the charge or current measurements, the effective collecting volume, ion recombination within the chamber, and changes in measured results due to chamber polarity differences. In their Table 8, these uncertainties were added in quadrature for a combined Type A standard uncertainty of 0.054%. In total, the Type B standard uncertainties were 0.316%, and included key components such as electric field distortion, mean energy per ion pair (i.e.,  $W/e$ ), and  $k_{att}$ . In combination, the total standard uncertainty was 0.32% for measurements at NIST of  $\dot{K}_{air}(d = 50 \text{ cm})$ . Given the inherent differences in methods between the experimental measurements and the simulations in the current study, the uncertainty analysis below is independent from those examined by Seltzer *et al.*<sup>4</sup>

Hiatt *et al.* identified and quantified the uncertainty components for simulations of the dose rate in water at distances of 1 cm and 5 cm from the model S700 eBT source.<sup>6</sup> Many of these uncertainty components were applicable to the current study for derivation of  $\dot{K}_{air}(d = 50 \text{ cm})$ . The uncertainties for the current study include the following:

a) Source construction: Based on dimensions provided by the manufacturer of the model S700 source, a maximum tolerance of 50  $\mu\text{m}$  was specified for individual source components, except for the W-alloy coating the anode interior where most measurements of the film thickness are in the range of 0.7  $\mu\text{m}$  to 0.9  $\mu\text{m}$ , and the anode thickness, which had a 25  $\mu\text{m}$  (0.001") tolerance.<sup>25</sup> As the W-alloy coating thickness is near that which maximally produces bremsstrahlung x rays (results not shown), coating thicknesses in this range would alter the tube output by about 1%, which was similar to that observed by others.<sup>26,27</sup> Tube output changed inversely with anode thickness in the range of 0.356 mm. Assuming a normal distribution with a standard deviation of 0.1  $\mu\text{m}$  for the coating thickness uncertainty and a rectangular distribution for measured anode thickness

uncertainty,<sup>25</sup> a Type B standard uncertainty of 5.4% was assigned for derivation of  $\dot{K}_{air}(d = 50 \text{ cm})$ .

- b) Dynamic internal components: As described by Hiatt *et al.*,<sup>6</sup> the plastic centering insert decreases anode motion within the tube sheath, with a maximum potential movement estimated to be  $\pm 0.02 \text{ cm}$ . Using a rectangular distribution for this uncertainty component, a Type B standard uncertainty of 0.05% was estimated for  $d = 50 \text{ cm}$ .
- c) Source spectrum: The Xoft high voltage controller maintains the operating voltage within 0.2 kV (0.4%) of 50 kV and within 2  $\mu\text{A}$  (0.7%) of 300  $\mu\text{A}$ .<sup>25</sup> At  $d = 50 \text{ cm}$  in air, a Type B standard uncertainty of 0.48% was estimated using a rectangular distribution for these constraints.
- d) Air attenuation within the chamber: The  $k_{att}$  correction factor was determined by assessing the change in air kerma as a function of distance within the Lamperti chamber. Uncertainties in this method included the tally statistics and uncertainties in fitting results to exponential attenuation given the narrow-beam geometry. A Type B uncertainty of 0.14% was estimated for derivation of  $\dot{K}_{air}(d = 50 \text{ cm})$ .
- e) Air scatter: As stated in Sec. 2.C.1, the value for  $k_{sc}$  was taken from Seltzer *et al.*,<sup>4</sup> as was a standard uncertainty of 0.03%.
- f) Cross sections: MCNP6 was selected as the main computational tool in this study as it offered improvements in the coupled electron and photon transport capabilities over MCNP5.<sup>10</sup> The MCNP6 code includes sub-shell specific photoelectric data and more accurate photoelectric absorption and photoelectron generation.<sup>9</sup> An uncertainty of 0.5% was estimated for the pertinent electron cross-sections. An uncertainty of 0.62% was estimated for  $\mu_{en}/\rho$  to derive air-kerma rate.<sup>28</sup> Also notable was the uncertainty in the log-log interpolation used by MCNP6 for  $\mu_{en}/\rho$  values from the NIST database as input by the user as the DE DF cards.<sup>22</sup> In his dissertation work, Davis found an 11% error in  $\mu_{en}/\rho$  estimation at  $\sim 70 \text{ keV}$ .<sup>21</sup> Given the lower maximum energy and broad spectrum for the model S700 source, an uncertainty of 0.5% was estimated for the current study. Taking these three components in quadrature combination, a total Type B uncertainty of 0.9% was estimated for cross section-related uncertainties.
- g) Tally volume averaging: Dependence of  $\dot{K}_{air}(d = 50 \text{ cm})$  as a function of polar angle was small, and varied by approximately  $-0.7\%$  per degree at  $90^\circ$ . Given the 0.5 cm ( $0.6^\circ$ ) aperture of the NIST Lamperti chamber, a Type B standard uncertainty of 0.0002% was estimated. Due to the chamber design and collimation of the collecting volume, contributions due to tally volume averaging in the radial direction were considered negligible.
- h) Physics of MC code: The MCNP code is well established and has been compared to results from other codes for brachytherapy sources of similar energy to produce agreement of dose rate at 1 cm and 5 cm to within 0.1%.<sup>29</sup> However, that study was restricted to comparing codes only with photon transport. Unlike radiation transport simulations in water for determining the TG-43 brachytherapy dosimetry parameters where photon interactions in medium dominate, simulations of air-kerma rate are more dependent on the accuracy of electron transport and interactions such as bremsstrahlung on the source anode. As described in Sec.

2.A, a larger standard uncertainty (4%) in  $\dot{K}_{\text{air}}(d = 50 \text{ cm})$  derivation was estimated for this uncertainty component.

- i) Tally statistics: A total of  $10^{11}$  histories were simulated for the NIST Lamperti chamber, which resulted in a Type A standard uncertainty of 0.14%.

While the  $k_{\text{vol}}$  correction factor was used in Eq. (1) to determine  $\dot{K}_{\text{air}}(d = 50 \text{ cm})$ , its uncertainty was assumed to be zero given that any small dimensional variations would cancel out for derivation of this factor. As shown in Table I, the combined Type A and Type B standard uncertainties were 0.14% and 6.8%, respectively, which added in quadrature for a total standard uncertainty of 6.8%. Clearly, the uncertainty in  $\dot{K}_{\text{air}}(d = 50 \text{ cm})$  was dominated by the uncertainties in source geometry and the physics of the MC code due to the increased importance of electron transport in air simulations. The magnitude of this uncertainty differs from that determined by Safigholi *et al.*<sup>26</sup> and Hiatt *et al.*<sup>6</sup> as the air-kerma rate is an absolute metric in terms of tube current while the TG-43 dosimetry parameters determined by Safigholi *et al.* and Hiatt *et al.* were relative metrics.

Most of the uncertainty components identified by Seltzer *et al.*<sup>4</sup> were omitted from the analysis in the current study due to their reliance on measurement methods or having negligible values. For example, NIST had to estimate the uncertainties in air density and humidity given their measurements did not occur in dry air or at a reference temperature (22° C) and pressure (101.325 kPa). With MC simulations, the desired conditions are explicitly modeled and therefore are not subject to uncertainties. Similarly, other uncertainties included by NIST for their measurements with the Lamperti chamber were ion recombination, electron loss, electric field distortion, and polarity. These uncertainty components were excluded from the analysis in the current study given the methodology used to derive  $\dot{K}_{\text{air}}(d = 50 \text{ cm})$  in Eq. (1). Seltzer *et al.* estimated Type B uncertainties of 0.03% for photon scatter and 0.10% for diaphragm scatter. Due to the assumed equivalence of collisional kerma and absorbed dose, uncertainties in diaphragm scatter were considered negligible.

**Table I.** Components of an uncertainty analysis for MC simulations of the NIST Lamperti ionization chamber to determine  $\dot{K}_{\text{air}}(d = 50 \text{ cm})$  for the model S700 eBT source.

Uncertainty component	Type A (%)	Type B (%)
Source construction		5.4
Dynamic internal components		0.05
Source spectrum		0.48
Air attenuation		0.14
Air scatter		0.03
Cross sections		0.9
Tally volume averaging		<0.01
Physics of MC code		4
Tally statistics	0.14	
Quadrature sum	0.14	6.8
Total standard uncertainty		6.8

## 3. RESULTS

### 3.A. Lamperti chamber simulations

Using Eq. (1),  $\dot{K}_{\text{air}}(d = 50 \text{ cm})$  was estimated as  $(1.850 \pm 0.126) \times 10^{-4} \text{ Gy/s}$ . A value of  $k_{\text{att}} = 1.0083$  was obtained for radiation attenuation within the chamber narrow-beam geometry by traversing 4.0 cm in air.

### 3.B. Simulations in air

The raw MC outputs in air at  $\theta = 90^\circ$  were  $6.326 \times 10^{-10} \text{ MeV/(g-history)}$ ,  $5.378 \times 10^{-10} \text{ MeV/(g-history)}$ ,  $1.468 \times 10^{-10} \text{ MeV/(g-history)}$ , and  $6.050 \times 10^{-11} \text{ MeV/(g-history)}$  at 50, 54, 100, and 150 cm, respectively. The air-kerma rate at 50 cm for the S700 eBT source in air operating at 300  $\mu\text{A}$  was determined to be  $1.898 \times 10^{-4} \text{ Gy/s}$ . This value was 2.6% higher than for the Lamperti chamber, which had narrow-beam geometry where radiation scatter was excluded. After accounting for the expected decrease due to inverse-square, the air-kerma rate decreased linearly as a function of distance from the source.

A decrease in photon fluence was observed (Fig. 3(a)) for  $\theta > 148^\circ$  due to the attenuation through the Kovar sleeve and the Ag epoxy components.<sup>6</sup> As a result of interactions with Cu, Y and Ag, characteristic x-ray photopeaks were observed and attributed to Cu for  $\text{KM}_{2,3} = 8.9 \text{ keV}$ , Y for  $\text{KL}_{2,3} = 14.9 \text{ keV}$  and  $\text{KM}_{2,3} = 16.7 \text{ keV}$ , and Ag for  $\text{KL}_{2,3} = 22.1 \text{ keV}$ ,  $\text{KM}_{2,3} = 24.9 \text{ keV}$ , and  $\text{KN}_{2,3,4,5} = 25.5 \text{ keV}$ .<sup>30</sup> Photon fluence decreased for spectral curves with  $\theta \geq 150^\circ$  and was attributable to the Y K-edge caused by the photons traversing the anode. The Ag K-edge (25.5 keV) was not observed for  $\theta < 150^\circ$  where only the atomic transitions were observed.

### 3.C. Simulations in vacuum

The raw MC outputs in vacuum at  $90^\circ$  were  $6.826 \times 10^{-10} \text{ MeV/(g-history)}$ ,  $5.842 \times 10^{-10} \text{ MeV/(g-history)}$ ,  $1.703 \times 10^{-10} \text{ MeV/(g-history)}$ , and  $7.568 \times 10^{-11} \text{ MeV/(g-history)}$  at 50, 54, 100, and 150 cm, respectively. As expected, results scaled according to the inverse square of the distance. The air-kerma rate at 50 cm for the S700 eBT source in vacuum operating at 300  $\mu\text{A}$  was determined to be  $2.048 \times 10^{-4} \text{ Gy/s}$ . This value was 7.9% higher than the broad-beam in-air results and was attributed to photon attenuation in air, especially for the low-energy photons that are challenging to simulate and to account for with measurement techniques.

Fig. 3(b) depicts the photon spectra as a function of polar angle and photon energy at a distance of 50 cm in vacuum. The most striking aspect of the plot was the influence of the Kovar sleeve, brass washer, and Ag epoxy components were observed at  $\theta > 148^\circ$  and  $E_\gamma = 25.7 \text{ keV}$  where the Ag K-edge caused a decrease in photon intensity. Observable across all polar angles are the photo peaks at 8.0 keV and 8.9 keV caused by photon interactions with Cu, a component of the brass washer located proximal to the anode, and peaks at 14.9 keV and 16.7 keV caused by photon interactions with Y, an anode component. Photons from the lower polar angles contributed to increased scatter at the higher polar angles for the in-air simulations as compared to the in-vacuum simulations for which no scattering existed. Increased incoherent scattering was observed at polar angles in the region of the attenuating Ag epoxy and resulted in blurring of this physical edge due to scattered photons as was observed in the dark blue region above 25 keV and  $150^\circ$  in

Fig. 3(a). A marked reduction in photon fluence as a function of polar angle was also observed at the Ag K-edge with a greater difference between the 135° to 150° curves than for the curves for curves  $\theta \leq 135^\circ$ .

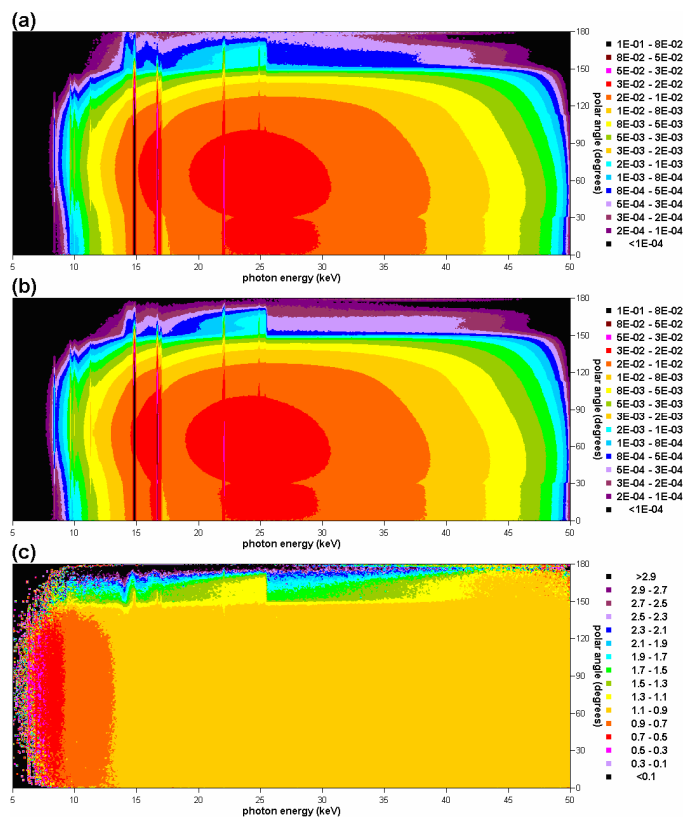


**Fig. 3.** Photon fluence (arbitrary units) as a function of photon energy and polar angle at  $d = 50$  cm in (a) air and (b) vacuum within a 200 cm radius sphere with the condensed history method. The maximum fluence in both phantoms was observed at  $\theta \sim 70^\circ$  as supported by results in Fig. 3. Also evident were the characteristic x ray photopeaks at 8.4, 9.7, 10.0, and 11.3 keV that were attributed to W; 14.9, 16.7, and 17.0 keV that were attributed to Y; and 22.0 and 24.9 keV that were attributed to Ag. Also, the K edge for Y was observed at 17.0 keV for  $\theta < 150^\circ$  where the anode was present, and for Ag at 25.5 keV for  $\theta > 148^\circ$  where the Ag epoxy was present. (c) ratio of photon fluences (with the same normalizations) for air to vacuum were within 10% of unity for most of the polar angles and photon energies, with decreases beneath 13 keV attributed to photon attenuation in air. Also evident was the Ag K edge for  $\theta > 150^\circ$  due to photon scattering in air, which did not occur in vacuum.

#### 4. DISCUSSION

The primary objective of this investigation was to independently model the calibration geometry used at NIST to measure the air-kerma rate for the model S700 eBT sources. A downside to measurements of a desired quantity is the need to apply correction factors to compensate for physical effects that influence the measurement environment. These effects include phenomena such as radiation scatter in the medium and by the measurement apparatus, uncertainties in ascribing compositions for the existent materials, and deficiencies in the chamber operation characteristics from an ideal detector. The MC approach employed in this work allowed for simulation of the calibration geometry without the need to apply the many correction factors required for the experimental measurements and provides the first published air-kerma rate evaluation for the model S700 eBT

source. This study provides a theoretical assessment of air-kerma rate. Both narrow beam and broad beam geometries were modeled. Benefits of additionally simulating the broad beam geometry were that there were no secondary effects to consider such as interactions within chamber materials or arbitrary dimensions attributed to the measurement calibration geometry, and also the broad beam results in air and in vacuum served to provide a sanity check of the results for the simulated geometry of the Lamperti chamber. Differences between results obtained for the three geometries were of the expected magnitude. A key finding was that the air-kerma rate value from the current study, which fell within the range observed by NIST, served to substantiate the NIST measured air-kerma rate data and their calibration methodology. However, enthusiasm for this finding must be tempered when considering that source output is dependent on the nominal tube current and subtle differences in source design. This is discussed further in Sec. 4.A.

Users of clinical eBT systems calibrate their sources through a NIST traceable calibration of their reentrant well-type air ionization chamber. In clinical settings, a well chamber with an Al insert is used for pre-treatment calibration. The well chamber used for clinical calibrations is sent to an ADCL offering the eBT calibration service. An eBT source is inserted into the clinical well chamber, then compared to the well chamber response (for the same source) that was calibrated at NIST based on the Lamperti calibration standard.

Through establishing an air-kerma rate calibration standard for eBT sources as opposed to the air-kerma strength calibration standard,<sup>4</sup> DeWerd *et al.* identified necessary changes in the TG-43 dose calculation formalism for brachytherapy dosimetry.<sup>7</sup> In their modified protocol for eBT dosimetry, DeWerd *et al.* suggested replacing the TG-43 dose-rate constant with a dose-rate conversion coefficient  $\chi_i$  where  $i$  represents the applicator material with  $i = 0$  referring to the bare source and  $\chi_0$  defined as the ratio of the dose-rate at 1 cm in water along the source transverse plane (i.e., the reference position) to the air-kerma rate at 50 cm. Based on the dose-rate value of  $(1.006 \pm 0.017) \times 10^5$  cGy/h in water at the reference position from Table I of Hiatt *et al.*<sup>6</sup> (recalculated using MCNP6, the default DBCN(18) energy indexing, and the EPRDATA12 photoatomic cross section library), with the denominator being the  $\dot{K}_{\text{air}}(d = 50 \text{ cm})$  value determined in the current study, a value of  $\chi_0 = 1,511 \pm 106$  was determined for the model S700 eBT source. A value of 0.60 was obtained when correcting  $\chi_0$  by the inverse-square for a common distance of 1 cm. This value is similar to the dose-rate constant for <sup>103</sup>Pd seeds, which have similar photon energies as the model S700 eBT source.<sup>2,6</sup>

The methods in this study permitted evaluation of spectral results in both air and vacuum at identical locations. Investigation (results not shown) of the eBT photon spectrum across all polar angles at a distance of 50 cm in air and vacuum were the same within 10%, except in regions where attenuation and scatter played a significant role. In the region below 13 keV, the ratio of photon fluence in-air to in-vacuum was decreased at all polar angles due to attenuation of the photons in air. In the region for  $\theta > 150^\circ$ , enhanced scatter from the Kovar sleeve and Ag epoxy components resulted in an increased ratio of air to vacuum.

#### 4.A. Comparison with NIST

For three different model S700 sources, NIST obtained a mean value of  $\dot{K}_{\text{air}}(d = 50 \text{ cm}) = 1.91 \times 10^{-4} \text{ Gy/s}$ .<sup>23</sup> This value was 3.3% larger than the one determined in the current study using MC simulation methods. While this difference was less than the total uncertainty of 6.8% determined in Table I, the  $\dot{K}_{\text{air}}(d = 50 \text{ cm})$  measurements at NIST spanned a range of  $0.44 \times 10^{-4} \text{ Gy/s}$ , or 23% of the mean, which encompassed the simulated result. This magnitude of source output variation agrees with the 30% level observed by Davis.<sup>21</sup> For the Lamperti chamber from Table 8 in Seltzer *et al.*,<sup>4</sup> the combined total (Type A + Type B) standard uncertainty (percent) was  $(0.15^2 + 0.316^2)^{1/2} = 0.35\%$ . Therefore, the measured uncertainty in  $\dot{K}_{\text{air}}(d = 50 \text{ cm})$  was much smaller than the observed variation across tubes, and also smaller than the uncertainties associated with the current study.

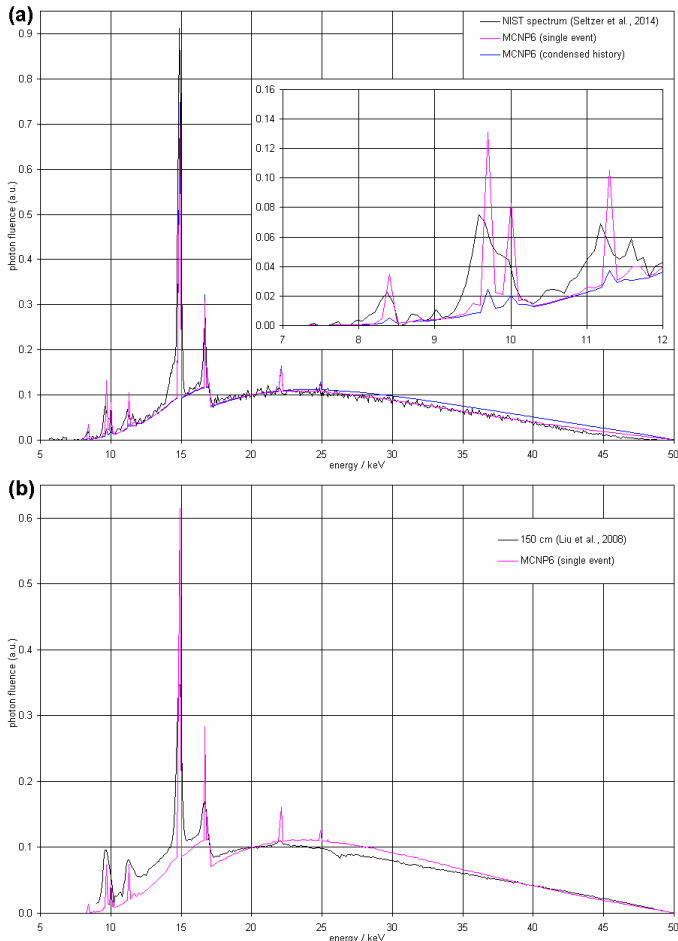


**Fig. 4.** (a) The photon spectra on the transverse plane of the model S700 eBT source at a distance of 50 cm in air from NIST using a HPGe detector,<sup>4,31</sup> and from simulations using the MCNP6 code with various physics models. Unlike the condensed history method, the single event method included electron impact ionization for generating W L-edge characteristic x rays as shown in the inset. (b) Spectra were also simulated at 150 cm for direct comparison to measurements using a CdTe detector by Liu *et al.*<sup>32</sup> All spectra were normalized to a value of 0.1 at 20 keV. The energy bins were 0.081 keV for the NIST spectrum and 0.1 keV for the MCNP6 spectra and for Liu *et al.* The most prominent peaks were at 14.9 keV and 16.7 keV, with the Y K-edge (17.0 keV) also evident.

At NIST, measured and calculated values of 1.0083 and 1.0087 for  $k_{\text{att}}$  traversing 4.0 cm in air were reported in the paper by Seltzer *et al.*<sup>4</sup> Our simulation result of  $k_{\text{att}} = 1.0083$  was identical to that measured by NIST and within its uncertainties (0.14%) for their calculated result. The photon spectrum reported by Seltzer *et al.*<sup>4,31</sup> of NIST at 50 cm in air on the transverse plane of the model S700 eBT source was compared at the same position to the simulated results in air as shown in Fig. 4(a). A low-energy cutoff of approximately 8 keV was observed in the measured and simulated spectra,<sup>4</sup> and was attributed to photon attenuation in the source and the 50 cm of air in front of the collecting volume. Spectral peaks associated with elements comprising the model S700 source were visible in all spectra. In the 8 keV to 12 keV energy range, there was a discrepancy in photopeak magnitude between the measured and simulated (condensed history) spectrum. The W photopeaks from  $L_3M_5$ ,  $L_2M_4$ , and  $L_3N_5$  transitions were higher in the measurement setting, but with similar areas as those generated using the single-event electron physics models.

#### 4.B. Comparison with Liu *et al.*

In 2008, Liu *et al.* published a spectroscopic characterization of the model S700 eBT source.<sup>32</sup> They measured the source photon spectrum at operating voltages of 40 kV and 50 kV using a model XR-100T (Amptek Inc., Bedford, MA) CdTe spectrometer positioned 150 cm from the source. The spectrometer measurements were corrected for detector response. Their 50 kV spectral data is plotted alongside MCNP6 results also at 150 cm in Fig. 4(b). The W and Y photopeaks were in alignment. The Liu *et al.* spectrum exhibited a spectral deficit at 27 keV, and their fluence results for  $< 18 \text{ keV}$  were noticeably higher than our simulated results, in contrast to the NIST spectrum.<sup>4</sup> Like the NIST spectrum, the Liu *et al.* spectrum did not portray the Ag photopeaks as shown in the simulated results.

#### 4.C. Study limitations

While the source was modeled according to the most recent design information available, knowledge of the true source geometry and the electron fluence impinging on the anode were considered to be the major limitations of this study. Simulations in the current study did not include an electric field for generating the 50 kV potential, which may cause electron paths within the tube to differ from the simulations. For components that were able to be physically measured (e.g., outer catheter sheath and plastic centering insert), their dimensions were confirmed by caliper measurements with an accuracy of approximately 0.1 mm. A shortcoming of this study was that the dimensions of small components, such as the micrometer-thick W-alloy coating the anode interior, were not able to be directly confirmed with those dimensions reported by the manufacturer. Uncertainties in the exact shape of some internal components such as the Ag epoxy, which is manually painted on the eBT tube, may be the cause of the spectral discrepancies.

Another study limitation was the assumption of azimuthally symmetry for the spherical air and vacuum substudies. Most source components were azimuthally symmetric and their rotational orientation therefore would not matter. However, the anode centering insert has a clover-leaf shape and was not azimuthally symmetric. The insert's shape is so complex that other investigators have simulated it as a simple right cylinder.<sup>21</sup> To investigate the importance of the orientation of this

component, Hiatt *et al.*<sup>6</sup> showed that the influence of the azimuthally-asymmetric anode centering insert orientation was less than 1%. To mitigate this phenomenon and azimuthally-asymmetric source output variations due to other reasons, the NIST calibration standard averages three air-kerma rate measurements at varying azimuthal angles (i.e., 0°, 120°, and 240°). Given that the orientation of the insert is unknown during an air-kerma rate measurement or a clinical treatment, the azimuthal asymmetry of the source was not considered further.

A limitation of the method for converting the simulated kerma within the Lamperti chamber to air-kerma rate was reliance on the 300  $\mu\text{A}$  beam current for normalization. There can be a considerable output variation of the S700 source due to differences in target manufacturing, electrons not hitting the target, and variations in source controllers to deliver the 300  $\mu\text{A}$ .<sup>21</sup> A possible method to obviate this issue would be to benchmark the Lamperti chamber model by simulating the relative responses of the Lamperti chamber and a well-type air ionization chamber.

#### 4.D. Future work

The MCNP6 radiation transport code has many improvements over the MCNP5 code, including a reworking of the coupled electron/photon transport capability to include electron and photon interactions, and atomic relaxation data from the 8<sup>th</sup> release of the 6<sup>th</sup> version of the Evaluated Nuclear Data File (ENDF/B-VI.8). A major goal of the MCNP6 upgrade was to allow coupled electron/photon transport down to 1 eV for photons and 10 eV for electrons. The ENDF/B-VI.8 database includes subshell-specific photoelectric and electroionization cross sections. With MCNP6, photoelectron generation and the subsequent relaxations are managed more precisely and with enhanced detail than MCNP5. Previous versions of the MCNP code only considered K shell relaxations and weighted averages of the L shells with a maximum of five transitions. Consequently, discrepancies were observed between the different MC radiation transport codes, e.g., EGSnrc and PENELOPE.<sup>21</sup> The new information provided in the ENDF/B-VI.8 database allows the MCNP6 radiation transport code to now handle up to 29 subshells

and nearly 3,000 distinct transitions. Future work could include the collaboration of research groups proficient in differing radiation transport codes to consistently model an eBT source and explore the differences observed between the codes.

## 5. CONCLUSIONS

Through MC simulations of radiation transport, this study independently validated the  $\dot{K}_{\text{air}}(d = 50 \text{ cm})$  values measured at NIST for the model S700 eBT source. The results were in agreement within 8%. This difference was smaller than the range (i.e., 12%) of the measured values. As for the NIST measurement setup of the eBT source positioned between the Lamperti ionization chamber and the HPGe spectrometer, the generated photon spectrum was also evaluated in this study. When analyzing the spectrum as a function of polar angle, the influence of the Ag epoxy was readily observed through a marked reduction in output for  $\theta > 150^\circ$ . On the transverse plane, the simulated spectrum was in good agreement with the measured spectrum from NIST except for photons greater than 35 keV.

## ACKNOWLEDGEMENTS

The authors thank Linda Kelley and Tom Rusch of Xoft, Inc. (a subsidiary of iCAD, Inc.) for providing design information and physical samples for determining the dimensions of the model S700 electronic brachytherapy source. We also extend our appreciation to Michelle O'Brien and Michael Mitch of the National Institute of Standards and Technology for providing details on the electronic brachytherapy source calibration standard. Frank Verhaegen of the Maastricht Clinic in the Netherlands provided measured spectral data from Liu *et al.* Stephen Davis of McGill University has contributed to writing some of this work, our understanding of the MCNP6 code, and potential discrepancies with reality. Finally, Wesley Culberson and Larry DeWerd of the University of Wisconsin have reviewed a preliminary version of this paper with an eye towards facilitating practical issues on source calibrations and tube output normalization to the 300  $\mu\text{A}$  nominal tube current.

## REFERENCES

- 1 M. J. Rivard, S. D. Davis, L. A. DeWerd, T. W. Rusch, and S. Axelrod. "Calculated and measured brachytherapy dosimetry parameters in water for the Xoft Axxent X-Ray Source: an electronic brachytherapy source," *Med. Phys.* **33**, 4020–4032 (2006).
- 2 M. J. Rivard, B. M. Coursey, L. A. DeWerd, W. F. Hanson, M. S. Huq, G. S. Ibbott, M. G. Mitch, R. Nath, and J. F. Williamson, "Update of AAPM Task Group No. 43 report: A revised AAPM protocol for brachytherapy dose calculations," *Med. Phys.* **31**, 633–674 (2004).
- 3 L. A. DeWerd, M. S. Huq, I. J. Das, G. S. Ibbott, W. F. Hanson, T. W. Slowey, J. F. Williamson, and B. M. Coursey, "Procedures for establishing and maintaining consistent air-kerma strength standards for low energy, photon-emitting brachytherapy sources: Recommendations of the Calibration Laboratory Accreditation Subcommittee of the American Association of Physicists in Medicine," *Med. Phys.* **31**, 675–681 (2004).
- 4 S. M. Seltzer, M. O'Brien, and M. G. Mitch, "New national air-kerma standard for low-energy electronic brachytherapy sources," *J. Res. Natl. Bur. Stand.* **119**, 554–574 (2014).
- 5 M. Boutillon, W. H. Heney, and P. J. Lamperti, "Comparison of exposure standards in the 10-50 kV x-ray region," *Metrologia* **5**, 1–11 (1969).
- 6 J. R. Hiatt, S. D. Davis, and M. J. Rivard, "A revised dosimetric characterization of the model S700 electronic brachytherapy source containing an anode-centering plastic insert and other components not included in the 2006 model," *Med. Phys.* **42**, 2764–2776 (2015).
- 7 L. A. DeWerd, W. S. Culberson, J. A. Micka, and S. J. Simiele, "A modified dose calculation formalism for electronic brachytherapy sources," *Brachytherapy* **14**, 405–408 (2015).
- 8 T. Goorley, M. James, T. Booth, F. Brown, J. Bull, L. J. Cox, J. Durkee, J. Elson, M. Fensin, R. A. Forster, J. Hendricks, H. G. Hughes, R. Johns, B. Kiedrowski, R. Martz, S. Mashnik, G. McKinney, D. Pelowitz, R. Prael, J. Sweezy, L. Waters, T. Wilcox, and T. Zukaitis, "Initial MCNP6 release overview," *Nucl. Technol.* **180**, 298–315 (2012).
- 9 H. G. Hughes, "An electron/photon/relaxation data library for MCNP6," Los Alamos National Laboratory Report No. LA-UR-13-27377, Los Alamos, NM, September 23, 2013.
- 10 H. G. Hughes, "Enhanced electron-photon transport in MCNP6," Los Alamos National Laboratory Report No. LA-UR-13-27632, Los Alamos, NM, October 27, 2013.

- <sup>11</sup> F. B. Brown, "Status of cross-section data libraries for MCNP," Los Alamos National Laboratory Report No. LA-UR-13-23040, Los Alamos, NM, April 29, 2013.
- <sup>12</sup> [Online] Available: <https://www-nds.iaea.org/public/download-endf/ENDF-B-VI-8/> International Atomic Energy Agency Nuclear Data Services, Vienna, Austria (accessed 2015 November 25)
- <sup>13</sup> D. E. Cullen, J. H. Hubbell, and L. Kissel, "EPDL97: The Evaluated Photon Data Library, '97 Version," Lawrence Livermore National Laboratory report UCRL-50400, Vol. 6, Revision 5 (September 19, 1997).
- <sup>14</sup> S. T. Perkins, D. E. Cullen, M. H. Chen, J. H. Hubbell, J. Rathkopf, and J. Scofield, "Tables and graphs of atomic subshell and relaxation data derived from the LLNL Evaluated Atomic Data Library (EADL), Z=1-100," UCRL50400, Vol. 30 (Oct. 31, 1991).
- <sup>15</sup> S. T. Perkins, D. E. Cullen, and S. M. Seltzer, "Tables and graphs of electron-interaction cross sections from 10 eV to 100 GeV derived from the LLNL Evaluated Electron Data Library (EEDL), Z=1-100," UCRL50400, Vol. 31 (Nov. 12, 1991).
- <sup>16</sup> H. G. Hughes, "Improved logic for sampling Landau straggling in MCNP5," Los Alamos National Laboratory Report No. LA-UR-05-4404, Los Alamos, NM, 2005.
- <sup>17</sup> S. D. Davis and L. A. DeWerd, "Monte Carlo study of an electronic brachytherapy source using MCNP5 and EGSnc," *Med. Phys.* **34**, 2472–2473 (2007) abstract.
- <sup>18</sup> D. R. Schaart, J. Th. M. Jansen, J. Zoetelief, and P. F. A. de Leege, "A comparison of MCNP4C electron transport with ITS 3.0 and experiment at incident energies between 100 keV and 20 MeV: Influence of voxel size, substeps and energy indexing algorithm," *Phys. Med. Phys.* **47**, 1459–1484 (2002).
- <sup>19</sup> R. A. Schwarz and L. L. Carter, "Visual Editor to create and display MCNP input files," *Trans. Amer. Nucl. Soc.* **77**, 311–312 (1997).
- <sup>20</sup> N. L. Gagne, K. L. Leonard, and M. J. Rivard, "Radiobiology for eye plaque brachytherapy and evaluation of implant duration and radionuclide choice using an objective function," *Med. Phys.* **39**, 3332–3342 (2012).
- <sup>21</sup> S. D. Davis, "Air-kerma strength determination of a miniature x-ray source for brachytherapy applications," Ph.D. Dissertation. University of Wisconsin-Madison (2009).
- <sup>22</sup> J. H. Hubbell and S. M. Seltzer. Tables of X-Ray Mass Attenuation Coefficients and Mass Energy-Absorption Coefficients (version 1.4) 2004. [Online] Available: <http://physics.nist.gov/xaamdi> National Institute of Standards and Technology, Gaithersburg, MD (accessed 2015 November 25).
- <sup>23</sup> Michelle O'Brien. Personal communication: January 7, 2014.
- <sup>24</sup> L. A. DeWerd, G. S. Ibbott, A. S. Meigooni, M. G. Mitch, M. J. Rivard, K. E. Stump, B. R. Thomadsen, and J. L. M. Venselaar, "A dosimetric uncertainty analysis for photon-emitting brachytherapy sources: Report of AAPM Task Group No. 138 and GEC-ESTRO," *Med. Phys.* **38**, 782–801 (2011).
- <sup>25</sup> Linda Kelley. Personal communication: September 21, 2015.
- <sup>26</sup> H. Safigholi, R. Faghihi, S. Karimi Jashni, A. S. Meigooni, "Characteristics of miniature electronic brachytherapy x-ray sources based on TG-43U1 formalism using Monte Carlo simulation techniques," *Med. Phys.* **39**, 1971–1979 (2012).
- <sup>27</sup> M. Khajeh and H. Safigholi, "Anode optimization for miniature electronic brachytherapy X-ray sources using Monte Carlo and computational fluid dynamic codes," *J. Advanced Res.* (in press) <http://dx.doi.org/10.1016/j.jare.2015.04.006>
- <sup>28</sup> P. Andreo, D. T. Burns, and F. Salvat, "On the uncertainties of photon mass energy-absorption coefficients and their ratios for radiation dosimetry," *Phys. Med. Biol.* **57**, 21172136 (2012).
- <sup>29</sup> M. J. Rivard, D. Granero, J. Perez-Calatayud, and F. Ballester, "Influence of photon energy spectra from brachytherapy sources on Monte Carlo simulations of kerma and dose rates in water and air," *Med. Phys.* **37**, 869–876 (2010).
- <sup>30</sup> R. D. Deslattes, E. G. Kessler Jr., P. Indelicato, L. de Billy, E. Lindroth, J. Anton, J. S. Coursey, D. J. Schwab, C. Chang, R. Sukumar, K. Olsen, and R. A. Dragoset. X-ray transition energies (version 1.2) 2005. [Online] Available: <http://physics.nist.gov/XrayTrans> National Institute of Standards and Technology, Gaithersburg, MD (accessed 2015 November 25).
- <sup>31</sup> Michael Mitch. Personal communication: May 12, 2015.
- <sup>32</sup> D. Liu, E. Poon, M. Bazalova, B. Reniers, M. Evans, T. Rusch, and F. Verhaegen, "Spectroscopic characterization of a novel electronic brachytherapy system," *Phys. Med. Biol.* **53**, 61–75 (2008).